Journal of Medicinal Chemistry

University of Sussex

Subscriber access provided by University of Sussex Library

Article

Inhibition of calcium dependent protein kinase 1 (CDPK1) by pyrazolopyrimidine analogs decreases establishment and reoccurrence of central nervous system disease by Toxoplasma gondii.

Florentine U. Rutaganira, Jennifer Barks, Mary Savari Dhason, Qiuling Wang, Michael Steven Lopez, Shaojun Long, Joshua B Radke, Nathaniel G Jones, Amarendar R Maddirala, James W Janetka, Majida El Bakkouri, Raymond Hui, Kevan M. Shokat, and L. David Sibley

J. Med. Chem., **Just Accepted Manuscript** • DOI: 10.1021/acs.jmedchem.7b01192 • Publication Date (Web): 21 Sep 2017

Downloaded from http://pubs.acs.org on September 23, 2017

Just Accepted

"Just Accepted" manuscripts have been peer-reviewed and accepted for publication. They are posted online prior to technical editing, formatting for publication and author proofing. The American Chemical Society provides "Just Accepted" as a free service to the research community to expedite the dissemination of scientific material as soon as possible after acceptance. "Just Accepted" manuscripts appear in full in PDF format accompanied by an HTML abstract. "Just Accepted" manuscripts have been fully peer reviewed, but should not be considered the official version of record. They are accessible to all readers and citable by the Digital Object Identifier (DOI®). "Just Accepted" is an optional service offered to authors. Therefore, the "Just Accepted" Web site may not include all articles that will be published in the journal. After a manuscript is technically edited and formatted, it will be removed from the "Just Accepted" Web site and published as an ASAP article. Note that technical editing may introduce minor changes to the manuscript text and/or graphics which could affect content, and all legal disclaimers and ethical guidelines that apply to the journal pertain. ACS cannot be held responsible for errors or consequences arising from the use of information contained in these "Just Accepted" manuscripts.

ACS Publications

Journal of Medicinal Chemistry is published by the American Chemical Society. 1155 Sixteenth Street N.W., Washington, DC 20036

Published by American Chemical Society. Copyright © American Chemical Society. However, no copyright claim is made to original U.S. Government works, or works produced by employees of any Commonwealth realm Crown government in the course of their duties.

Jm-2017-01192g

Inhibition of calcium dependent protein kinase 1 (CDPK1) by pyrazolopyrimidine analogs decreases establishment and reoccurrence of central nervous system disease by *Toxoplasma gondii*.

Florentine U. Rutaganira[1], Jennifer Barks[2a], Mary Savari Dhason[2a], Qiuling Wang[2a], Michael S. Lopez[1b], Shaojun Long[2], Joshua B. Radke[2], Nathaniel G. Jones[2], Amarendar R. Maddirala[3]. James W. Janetka[3], Majida El Bakkouri[4], Raymond Hui[4,5], Kevan M. Shokat[1], and L. David Sibley[2*].

[1] Howard Hughes Medical Institute and Department of Cellular and Molecular Pharmacology, University of California, San Francisco, San Francisco, California 94158, USA

[2] Department of Molecular Microbiology, Washington University School of Medicine, St. Louis, MO, 63130, USA

[3] Department of Biochemistry and Molecular Biophysics, Washington University School of Medicine, St. Louis, MO, 63130, USA

[4] Structural Genomics Consortium, University of Toronto, MaRS South Tower, 101 College St, Toronto, ON, M5G 1L7, Canada

[5] Toronto General Hospital Research Institute, 200 Elizabeth St., Toronto, ON M5G 2C4, Canada

[a] contributed equally, listed alphabetically,

[b] Achaogen Inc. 1 Tower Place, #300, South San Francisco, CA 94080

*Corresponding author

Key words: Parasite, opportunistic pathogen, chronic infection, tissue cyst, bradyzoite, encephalitis, AIDS, protein kinase, ATP-binding pocket, structure activity relationship, pharmacokinetics, X-ray crystal structure,

ABSTRACT: Calcium dependent protein kinase 1 (CDPK1) is an essential enzyme in the opportunistic pathogen *Toxoplasma gondii*. CDPK1 controls multiple processes that are essential to the intracellular replicative cycle of *T. gondii* including secretion of adhesins, motility, invasion, and egress. Remarkably, CDPK1 contains a small glycine gatekeeper residue in the ATP binding pocket making it sensitive to ATP-competitive inhibitors with bulky substituents that complement this expanded binding pocket. Here we explored structure-activity relationships of a series of pyrazolopyrimidine inhibitors of CDPK1 with the goals of increasing selectivity over host enzymes, improving anti-parasite potency, and improving metabolic stability. The resulting lead compound **24** exhibits excellent enzyme inhibition and selectivity for CDPK1 and potently inhibited parasite growth in vitro. Compound **24** was also effective at treating acute toxoplasmosis in the mouse, reducing dissemination to the central nervous system, decreasing reactivation of chronic infection in severely immunocompromised mice. These findings provide proof of concept for the development of small molecule inhibitors of CDPK1 for treatment of CNS toxoplasmosis.

INTRODUCTION

Toxoplasma gondii is a widespread protozoan parasite of animals that causes zoonotic infections in humans. Although most human cases are well controlled, infection in immunocompromised patients leads to serious sequelae, including toxoplasmic encephalitis and pneumonia, which are life-threatening if not treated [1]. Although the advent of HAART therapy has reduced the frequency of toxoplasmosis as an opportunistic pathogen in developed countries, it is still a serious complication in many parts of the world where patients do not have adequate access to testing or treatment for HIV infection [2-5]. Additionally, toxoplasmosis can cause serious problems in organ transplant and cancer chemotherapy patients due to their immunocompromised status [6]. Furthermore, toxoplasmosis is a recognized cause of severe ocular disease in healthy adults in some locations such as Brazil [7].

Current therapy for toxoplasmosis is based on combination of pyrimethamine, which blocks dihydrofolate reductase (DHFR), and sulfadiazine, a folate antagonist. Collectively these drugs disrupt replication by inhibiting nucleic acid synthesis. This drug combination is efficacious in treating acute infection through blocking replication of tachyzoites. Unfortunately pyrimethamine is associated with several adverse side effects including anemia due to bone marrow suppression [8] and many patients experience allergic reactions to sulfonamide drugs [9]. Chronic infections caused by *T. gondii* are typified by slow growing bradyzoites that reside within thick-walled tissue cysts [10]. The emergence of bradyzoites upon cyst rupture is thought to give rise to daughter cysts that sustain the chronic infection and contribute to recurrence of actively replicating tachyzoites when the parasite reverts to the lytic form. Hence, treatments

that could block re-emergence from the tissue cyst, or block invasion of host cells by bradyzoites could interrupt this cycle and eliminate chronic infection. Unfortunately, current therapies that inhibit DHFR and antagonize the folate pathway are not effective at clearing chronic infection, as evidenced by the high relapse in immunocompromised patients when therapy is discontinued [9], presumably due to the slow and sporadic replication of bradyzoites [11].

One of the key steps in defining new leads for therapeutic intervention is to identify essential pathways that can be targeted by small molecules. One potential new target is that fulfills these criteria is calcium dependent protein kinase 1 (CDPK1) in *T. gondii* [12]. Genetic depletion or chemical inhibition of CDPK1 blocks adhesion secretion and compromises motility, cell invasion, and egress [12], thus demonstrating the essentiality of this target. The X-ray crystal structure of CDPK1 also revealed an unusual feature in the ATP-binding pocket where a glycine (G) residue occupies the gatekeeper position where there is normally a larger hydrophobic residue [13, 14]. The presence of G gatekeeper is entirely unprecedented in human kinases [15], and CDPK1 is the only kinase in *T. gondii* with this unusual feature [16]. As a consequence, CDPK1 is exquisitely sensitive to bulky ATP competitive inhibitors such as pyrazolopyrimidines (PP), which mimic the nucleotide binding interactions with the hinge region within the ATP-binding pocket and project bulky substituents into the expanded hydrophobic pocket created by the G gatekeeper [17, 18]. These features have been exploited to develop PP analogs that are potent inhibitors of CDPK1 in *T. gondii* [19-21], and the most promising of these compounds show good efficacy in mouse models of toxoplasmosis [22-24].

Our prior studies involving derivatives with substituents (R1) to the C3 position of the pyrazolopyrimdine (PP) core revealed the importance of the methylene linkage at C3 to confer flexibility of R1 substituent binding [23]. However, compounds with the methylene linkage overall were not stable in the presence of rat liver microsomes, potentially due to the methylene bridge being subject to cytochrome P450 metabolism. To address these deficiencies, we have more fully explored the design and synthesis of different heteroatom linkages at the C3 position and expanded the diversity of substituents at the R2 position. Collectively, these rationally driven modifications have identified new TgCDPK1 inhibitors with excellent potency in addition to improved selectivity, metabolic stability, and in vivo efficacy in controlling toxoplasmosis in the mouse.

RESULTS

Design and synthesis of new PP analogs targeting CDPK1

To identify compounds with improved metabolic stability that would also exploit structural differences between CDPK1 and hSrc active sites, we designed and synthesized a compound library containing varied functional groups at R1 attached to the C3 position of the PP core (Scheme 1). These were either linked to the core pyrazolopyrimidine or pyrrolopyrimidine scaffold via methylene or heteroatom linkages (X) in combination with *t*-butyl or various R2 groups at the N1 position (Scheme 1). The hSrc kinase was chosen for initial counter-screening because it contains a threonine (T) gatekeeper residue that represents one of the smallest amino acids found in native human kinases [15]. All compounds were synthesized using previously described

methods to form the pyrazolopyrimidine scaffold or with advanced pyrrolopyrimidine intermediates [25, 26]. Methods to generate compounds with methylene linkage at C3 have been previously reported [23] and heteroatom linkages were incorporated using established aryl coupling chemistry [27-30] (**Scheme 1**). Detailed procedures for chemical synthesis and compound characterization are presented in the supplementary information.

Analysis of new PP analogs modified at the R1 position

To develop a structure-activity relationship (SAR) profile, we investigated the effects of modifying the R1 group and different linkers to the core scaffold at position C3 in a series of compounds that contained *tertiary* butyl at the N1 position (**Figure 1A**). We tested compounds for their potency against CDPK1 in vitro, using an ELISA assay for phosphorylated substrate, described previously [23]. In parallel, we tested the inhibitors for their ability to inhibit parasite growth in vitro using a β-Gal expressing line of *T. gondii* to determine EC_{50} values, as described previously [23]. Finally, we screened each analog for stability in vitro in the presence of rat liver microsomes, as a surrogate for estimating in vivo metabolic stability.

Starting with parent compound **1,** replacement of the C3 methylene linker with an ether, thioether, or amine linkage improved metabolic stability for ether and amine linkages (**Figure 1A**). This result confirms XenoSite in silico predictions of metabolism at the methylene as in compound **1**, that is less likely with ether and amine linkages as in compounds **2 and 4** but is still possible with thioether linkages as in **3 (Supplementary Figure S1)** [31]. The thioether linkage was also associated with substantial loss of activity in the parasite inhibition assay (**Figure 1A**). We also

observed increased metabolic stability of the ether linkage over methylene for another compound set consisting of compounds **5, 6**. Analogs bearing halogen substitutions were generally more stable, especially in the presence of the ether linkage. The addition of some -*meta* substituents on the benzyl ring was associated with loss of metabolic stability, despite having an ether linkage, for example addition of the methoxy group in compound **9** and the methyl group for compound **10** (Figure 1A). Since the ether linkage generally improved metabolic stability while maintaining efficacy against parasite replication, we selected ether linkages for further optimization.

Structural interactions between PP compounds and CDPK1

To better understand the binding interactions of PP analogs and the CDPK1 enzyme, we solved a series of high–resolution co-crystal X-ray structures, using previously described methods [14]. The co-crystal structure of CDPK1 with the lead compound **1** revealed a characteristic hydrogen-bonding (H-bonding) pattern of interaction between the aminopyridine and the kinase hinge. More specifically, the primary amine at C4 of the PP core acts as a H-bond donor in an interaction with the backbone carbonyl of glutamate (E) 129, and the N5 in the PP core acts as a H-bond acceptor in an interaction with the backbone amide of tyrosine (Y) 131 (**Figure 1B**). Importantly, the co-crystal structures of compounds **1 - 4** bound to CDPK1 show that these modifications do not substantially change the binding conformations (**Figure 1C**). Key H-bonding interactions between the PP core and the hinge region are maintained with R1 occupying the hydrophobic pocket formed by the presence of the small G gatekeeper residue (**Figure 1C**).

Analysis of new PP analogs modified at the R2 position

Previous studies of PP analogs have shown that larger substituents are tolerated at the R2 position and can lead to gain of potency and selectivity for CDPK1 [21]. To explore the size tolerance within the CDPK1 pocket at this region, we generated a series of analogs with cyclic amines at R2 (**Figure 2A**). Structural studies have shown that methyl piperidine in the R2 is positioned to form a H- bond with glutamate (E) 135 in the ribose binding region of the ATP pocket of CDPK1 [19, 20]. A co-crystal structure of compound **13** confirmed this interaction is also present in the series studied here (**Figure 2B**). The piperidine is predicted to be protonated under physiological conditions and as shown in the co-crystal structure, the additional H likely forms a salt bridge with glutamine (E) 135 (Figure 2B). We explored a series of cyclic amines based on piperidine where we elucidated the importance of proper placement and direction of the amine to form the favorable charge-charge salt bridge interaction with E135. We found that any deviation from the piperidine of **13** in this series abrogated CDPK1 activity and decreased inhibition of parasite replication in culture (**Figure 2A**). Compounds **16** and **15**, which contain a tetrahydropyran and pyridine group, respectively, each significantly lost potency, emphasizing the key contribution of the H-bond donor of the piperidine (**Figure 2A**). On the other hand, all cyclic amines showed greatly enhanced stability in the rat liver microsome assay thus providing much support for further R2 modification as an approach to improving metabolic stability (**Figure 2A**).

In another series, we explored the combination of methyl piperidine at R2 together with the prior functional groups at R1 (**Figure 3A**). Consistent with findings above, the methyl piperidine containing analogs generally showed improved metabolic stability in comparison to their *t* -butyl counterparts (**Figure 1A, 3A**). For example, the presence of

the methyl piperidine in compound **17** could impart stability despite having a methylene linkage to C3 of the PP core (**Figure 3A**). Compounds with additional halogens in the benzyl ring at R1 gained further increases in microsome stability (e.g. **21** and **22**) (**Figure 3A**). Furthermore, there were no significant differences between pyrazolopyrimidine and pyrrolopyrimidine as the core scaffold as demonstrated by compounds **18** vs. **23** (**Figure 3A**).

Despite the reproducible ability of methyl piperidine to improve microsome stability throughout the entire series, this modification also resulted in reduced biochemical potency and ability to block parasite replication. Hence, incorporation of methyl piperidine at R2 results in a tradeoff between improved metabolic stability and loss in potency. This effect may be explained by the larger size of these inhibitors that may not be as easily accommodated in the CDPK binding pocket. The combination of ether linked R1 as –*m*-Cl with R2 piperidine as in compound **13** showed the largest improvement over parent compound **1** while retaining reasonable activity in both inhibition CDPK1 and parasite growth (Figure 3A)**.** In contrast, methylation of the piperidine nitrogen in compound 25 led to a loss in potency, further highlighting the importance of the H-bonding ability of the protonated amine (**Figure 3A**). Converting the piperidine to a 6-membered ring δ-lactam in compound **26** also lead to a loss in enzyme potency and a complete loss in anti-parasitic activity (**Figure 3A**). We also explored modifying the piperidine by addition of di-fluorine (di-F) -*meta* to the amine, as such modifications are known to favorably affect the properties of drug-like molecules [32]. The di-F modification in compound **24** vs. **13,** which both have ether-linked R1 substitutions to the PP core, slightly improved enzyme inhibition and anti-parasitic

activity (**Figure 3A**). A homology model of **24**, based on the co-crystal structure of compound **13** with CDPK1, suggests that the piperidine amine is still in an appropriate position to interact with E135 (**Figure 3B, Table 1)**. We also made a similar modification of di-F in a *-meta* position to the piperidine amine in compound **18** to generate the compound **28**, both of which have a thioether linkage connecting R1 to C3 in the PP core. Surprisingly in this case, the di-F modification reduced enzyme activity and greatly diminished anti-parasitic activity. Modification of R2 to contain a trifluormethylcyclopropyl moiety was also synthesized in an attempt to reduce metabolic instability, based on a previous study showing this modification can improve stability of biaryl compounds relative to those containing *t*-butyl [33]. This compound **27** lost potency (**Figure 3**), suggesting it does not optimally fit in the CDPK1 ATP binding pocket, moreover it did not improve stability, perhaps due to the methylene linkage of the trifluormethylcyclopropyl moiety to N1 of the core.

Inhibition of CDPK1 in vitro correlates with parasite growth inhibition

To compare the potency of all of the new PP analogs synthesized here, we plotted the $\log_{10}$ values for CDPK1 enzyme inhibition (IC_{50}) vs. $\log_{10}$ values for parasite growth inhibition (EC_{50}) (**Figure 4A**). Fitting these data with a linear regression analysis indicated a reasonable correlation ($r^2 = 0.58$), supporting the conclusion that the activity of these compounds against parasite growth stems largely from inhibition of CDPK1. However, the fact that this correlation is not higher suggests that *in vivo* potency is also affected by other factors including differences in cell permeability. Some inhibitors lie above the diagonal line, which represents a perfect correlation, indicating they are less potent in blocking parasite growth, perhaps due to differences in cell permeability or

efflux (**Figure 4A**). Among the most potent inhibitors was the initial lead **1**, and derivatives that contain an oxygen linkage at R1 (e.g. **2** and **10**), as well as those that contain the methyl-piperidine at R2 (e.g. **13**, **24**)(**Figure 4A**). Based on a combination of potency, selectivity and PK properties, we prioritized compounds and selected these five analogs for further study. Other compounds that were potent in both assays were deprioritized for lack of specificity (e.g. **4**) or lack of stability (e.g. **9**).

Metabolic stability and cellular update of PP analogs

To help choose PP analogs most likely to be active in vivo, we broadly examined the physical properties, metabolic stability in mouse liver microsomes, and cellular uptake of a select group of PP analogs (**Table1**). All compounds have modest cLogP values, consistent with their intermediate hydrophobicity, and are predicted to have relatively small total polar surface area, properties that should facilitate penetration of the CNS (**Table 1**). Consistent with the findings in rat liver microsomes, the ether linkage in compound **2** reduced metabolic clearance in mouse liver microsomes when compared to compound **1**, although both values are still relatively high (**Table 1**). Compound **10**, which had similar clearance to compound **1** in rat liver microsomes despite having an ether linkage, was more rapidly cleared in mouse liver microsomes (**Table 1**), suggesting the methyl group at C3 might be prone to metabolism. Stability was further improved when the R2 group was switched from *t-butyl* to methyl piperidine as in compounds **13** and **18**. However these latter two compounds, which contain a basic amine group that is charged a neutral pH, were also associated with substantial efflux in MDCK cells (**Table 1**). In addition to the many other useful aspects of fluorine substitutions in medicinal chemistry, in some contexts it has been shown to reduce the

basicity of proximal amines by lowering the pKa [34]. Accordingly, we modified the piperidine ring by addition of di-fluorine (di-F), a modification reduced the pKa and nicely eliminated the efflux problem (**24** and **28**; **Table 1**). However, metabolic stability was diminished by the di-F modification in these compounds. Analogs such as **1** showed high levels of plasma protein binding (PPB) (i.e. 99%), however this property was greatly reduced for compounds containing methyl piperidine or the di-F methyl piperidine (**Table 1**). Importantly, none of the PP analogs tested affected the growth of human foreskin fibroblasts (HFF) cells in vitro at 10 μM, indicating that they are not toxic to host cells (**Table 1**).

Analysis of target specificity of select PP analogs

To provide an assay for inhibitor selectivity we cloned a variant of human Src, which has a threonine (T) residue at the gatekeeper (c-Src allele), which provides for an intermediate level of sensitivity to pyrazolopyrimidine compounds [18]. Although the initial lead compound **1** potently inhibited hSrc, modification of the R1 linkage to the PP core via an ether or thioether at C3 led to greater selectivity (**Figure 1A**). Modification of R2 to include cyclic amines, including piperidine, also led to large increases in selectivity for CDPK1 over hSrc (**Figure 2A**). Although Src has been used as a surrogate for human kinases with intermediate sensitivity to PP analogs [19, 21], it is only one member of a diverse family of tyrosine kinases that differ substantially in their sensitivity to PP inhibitors [35]. As such, we profiled select inhibitors **1, 2, 13, and 24**, which marked key transitions in our SAR profile. We screened all four analogs at 1 μM against a broad panel of 489 wild type and disease-associated human kinases (**Figure 5**). Inhibitor selectivity increased along our SAR profile, starting from thirty-nine kinases that are

inhibited or displaced by compound **1** by over 50% to only one kinase (CK1ε) that was inhibited or displaced by **24** by over 50% (**Figure 5, Supplementary Table S2**). Although compounds **13** and **24** exhibited IC_{50} values of ≤ 100 nM at 2 μM ATP, these values were increased almost 10 fold in the presence of 100 μM ATP (Supplementary Table S2). Additionally, we profiled an earlier inhibitor 3-methyl-benzyl-PP (compound **1** in [23]) to compare our initial lead **1** in this prior series. We determined that the selectivity profile for both of these compounds was similar **(Supplementary Figure S3**), while selectivity was greatly increased for compounds **13** and **14**. Full inhibitor profiling data is provided in the supplementary information (**Supplementary Tables S3-S5**).

Potency of select PP analogs against ex vivo bradyzoites

Previous studies have emphasized the ability of PP analogs to block host cell invasion and egress by the rapidly growing tachyzoite stage of *T. gondii* [19, 21, 23]. To examine the ability of our PP inhibitors to block invasion of bradyzoites, we purified mature tissue cysts from the brains of chronically infected mice and treated them in vitro with selected PP inhibitors. We compared the effects of treatment for short intervals (i.e. 4 hr followed by wash-out and further culture in the absence of compound) vs. continuous treatment during a 10-14 day plaquing assay. Consistent with previous reports showing that treatment with pyrimethamine requires overnight treatment to be effective in blocking tachyzoite growth [36] we observed that short-term treatment with pyrimethamine had minimal effect on infection by bradyzoites while continuous treatment blocked plaque formation (**Figure 4B**). In contrast, the PP inhibitors showed good (e.g. **13**), or excellent (e.g. **1**, **24**), ability to block infection following even short-term incubation (**Figure 4B**). Because the compounds were only present during the initial interaction of

the parasite with the host cell monolayer, we interpret these results to indicate that PP inhibitors can block bradyzoite entry into host cells during the 4 hr treatment period, resulting in greatly diminished plaque formation. Additionally, continual culture with PP compounds resulted in greater inhibition (**Figure 4B**), consistent with its ability to block the multiple rounds of invasion and egress that occur during plaque formation, although it is likely that tachyzoites predominate during these longer-term assays.

Mouse pharmacokinetic studies

We examined the pharmacokinetics (PK) of several PP inhibitors in mice following either i.v. injection or p.o. administration in mice. Compounds **1** and **2** showed reasonable oral bioavailability (F) ranging from ~ 25-30%, Cmax levels, and moderate clearance (Cl) values that were below the level of single pass circulation through the liver in mouse (~90 ml/min/kg) (**Table 2**). Compound **10** showed a higher clearance rate, but had similar half-life ($T_{1/2}$) to **1** and **2** of ~ 1.5 to 2 hr (Table 2). However, this compound suffered from poor oral bioavailability (**Table 2**). Although compound **13** had greater in vitro stability in microsomes (**Table 1**), it also displayed rapid clearance in vivo, perhaps due to efflux as indicated above. Compound **13** also showed lower Cmax values and high tissue exposure as evidenced by its volume of distribution (Vss) (**Table 2**). Finally, compound **24** showed the best combination of properties with good CMax following oral dosing, moderate clearance rate, $T_{1/2}$ ~1.5 hr, and very high oral availability (e.g. ~ 94%) (**Table 2**). These collective properties of compound **24** provided the best PK profile and highest values for AUC, reflecting prolonged serum exposure following oral dosing.

Based on these favorable properties, we examined the PK of **24** in mice using increasing oral doses from 10, 25, and 50 mg/kg (**Figure 4C**). At higher does, **24** showed a two-phase decay curve in plasma, with rapid initial drop followed by a more gradual plateau that was seen at 25 and 50 mg/kg (**Figure 4C**). Based on its protein binding properties (12% free in serum), the concentration of compound **24** in serum would need to be 2.08 μM, for the free value to attain a level equivalent to the in vitro EC_{50} of ~0.250 μM. This corresponds to a value of 856 ng/ml in serum, as shown by the red line in **Figure 4C**. The protein bound fraction in brain was slightly higher at 97.2%, or 2.8% free, and the ratio of total compound in the CNS vs. serum was 5.6, for an effective brain vs. plasma ratio ~ 1.3. Consequently, we would expect that the brain free concentration of compound **24** in the brain was approximately the same or slightly higher than that shown for serum in **Figure 4C**.

Treatment of acute toxoplasmosis

Based on its favorable PK parameters, we tested compound **24** for its ability to prevent toxoplasmosis in the mouse model. Following an initial loading dose of 50 mg/kg, **24** was administered orally at 25 mg/kg BID for 6 days, beginning 24 hr after challenge with tachyzoites of the ME49 strain of *T. gondii*. Treatment with **24** decreased the frequency of lethal infection (**Figure 6A**), and this was associated with reduced weight loss (**Figure 6B**) and with decreased tissue burdens of the parasite, as revealed by bioluminescent imaging (**Figure 6C**). Consistent with a decrease in acute burden, there were fewer tissue cysts formed in the brains of chronically infected mice following treatment with **24** (**Figure 6D**). The dramatic ability of **24** to decrease dissemination was further shown by bioluminescent imaging, where control animals showed extensive

expansion of the parasite with in the peritoneum at day 8 and spread to the head at day 18 (**Figure 6E,F**). In contrast, treated mice were able to restrict the growth of the parasite to the site of injection and did not show detectable signal in the head (**Figure 6E,F**). Following treatment with **24**, many animals showed tissue cyst levels below the levels of detection (40 cysts per brain) (**Figure 6D**). These animals were subsequently bio-assayed by oral feeding of 20% of their brain homogenate into a naïve interferon gamma receptor knock out mouse (Ifngr1$^{-/-}$). Although 5 of 6 recipient animals succumbed to infection, reflecting a low level of chronic infection in the donor, one remained alive, indicating that compound **24** treatment had resulted in a complete cure in this animal (**Figure 6D**, red triangle).

Treatment of reactivated CNS toxoplasmosis

To determine whether compound **24** could prevent reactivation of chronic toxoplasmosis, we utilized mice lacking the IFNγ receptor (i.e. Ifngr1$^{-/-}$), which are highly susceptible and rapidly succumb to infection [37]. Treatment of such animals with sulfadiazine will suppress the growth of tachyzoites, while allowing the development of chronic tissue cysts [38]. Subsequent removal of sulfadiazine results in rapid reactivation, characterized by CNS encephalitis, pneumonia and death [38]. We injected Ifngr1$^{-/-}$ mice with a type II strain capable of causing chronic infection and treated them from day 2-22 with sulfadiazine in the drinking water, which prevented otherwise lethal infection. Following removal of sulfadiazine (48 hr later), mice were treated with compound **24** at a dose of 25 mg/kg or 40 mg/kg BID, or with vehicle only control, by oral gavage for 8 days (**Figure 7A**). Withdrawal of sulfadiazine from the control animals lead to rapid reactivation of chronic infection led to death of the control mice within 10 days (**Figure**

7B). In contrast, treatment with compound **24** prolonged survival (**Figure 7B**). We also monitored the progression infection using bioluminescence. At the beginning of the treatment period, all of the animals were negative for bioluminescence, consistent with the infection being chronic. Monitoring of the control animals revealed that reactivation was first centered in the CNS, with later spread to the lungs prior to death (**Figure 7C**). In contrast to the rapid expansion of parasites seen in control mice, the bioluminescence signal was muted in compound **24** treated mice, and reactivation was significantly delayed (**Figure 7C**). Consistent with this delay in reactivation, compound **24** treated mice survived significantly longer (**Figure 7B**). One animal treated with compound **24** at 25 mg/kg and two animals treated at 40 mg/kg remained negative for bioluminescence signals and survived for an additional 22 days after removal of compound (red triangles in **Figure 7B**). Subsequent bioassay of brain homogenates from these treated mice into naïve Ifngr1$^{-/-}$ mice did not result in transfer of infection, confirming that these animals had been cured (**Figure 7 B**).

DISCUSSION

In previous work, we demonstrated that PP inhibitors containing –*meta* chloro benzyl substituents at C3 of the PP core provide potent inhibition of CDPK1 in *T gondii* [36]. However, when coupled with isopropyl or *t*-butyl at R2, these compounds suffer from metabolic instability [36]. Our profiling of host kinases here also reveals that compounds like **1** lack specificity, and this is also likely true of other related derivatives that share this basic architecture. To alleviate this problem, we altered the linkage connecting R1 to C3 from a methylene to a heteroatom consisting of O, S, or N. An ether linkage

proved most optimal in increasing stability and selectivity, while compounds with a thioether linkage were typically less active and compounds with an amine linkage were less selective. The reasons for these differences are not exactly clear as co-crystal structures of these analogs showed very close overlap of the analogs in the binding pocket. The lower activity of the thioether linkage may relate to the bulkier nature of this atom within the linker, which is very close to the hinge region in the crystal structure. We have previously shown that even subtle modification to this linker, such as substitution of fluorine for hydrogen, ablates activity [23].

By combining the ether linkage at C3 with a methyl piperidine at R2, we achieved further gains in specificity, with only modest loss of potency. Other modifications to R2, such as including a pyridine or methylation of the piperidine nitrogen, ablated activity suggesting that the unsubstituted alkyl amine is critical for the potency. Indeed a co-crystal structure of compound **13** revealed this amine is important for forming a hydrogen bond with glutamate (E) 135 in the ribose-binding region, likely stabilizing the interaction of the compound with the ATP-binding pocket. Addition of the piperidine group in the scaffold described here also resulted in dramatic improvement in specificity over host kinases compared to the initial lead compounds **1** and **2**. Compounds **13** and **24** only potently inhibited a single human kinase CK1ε under conditions tested here. Surprisingly, CK1ε is also sensitive to other PP analogs including 1-NM-PP1 and 1-NA-PP1, despite its methionine (M) gatekeeper, which is normally a hallmark for resistance to such analogs [39]. The sensitivity of CKε to PP analogs has been attributed to an unusual flexibility in the M side-chain that allows access of bulky PP analogs into the ATP-binding pocket [40]. Further modification of the PP scaffold may result in inhibitors

that would retain potency for CDPK1 over CKε. However, this off target activity may be less of an issue in vivo since compound **24** retains good potency against parasite growth in a cell-based assay, while off target activity against CKε drops appreciably at higher ATP levels.

Despite the improvements in specificity achieved with the piperidine analogs, these charged primary amines suffered from efflux problems in our study, likely due to the high pKa [34]. Addition of di-F in the piperidine ring decreased the predicted pKa and eliminated the efflux problem, consistent with previous examples in other scaffolds [34]. Previous experimental measurements of piperidine amines with fluoro substituents [34], combined with computational predictions of the compound **24** piperidine amine pKa suggest that the piperidine amine in compound **24** is partially protonated at physiological pH. Based on these properties and its potency, we would predict that compound **24** is still able to form a H-bond with E135 in CDPK1. Unfortunately, modification of di-F *meta* to the amine in the piperdine was also associated with some loss of metabolic stability, which likely limited its in vivo efficacy. We did not explore modification with fluorine-directed modifications at other positions in the piperidine ring, but conceivably some of these may have a more optimal combination of features.

One of the goals of our study was to obtain molecules with better metabolic stability to improve in vivo PK properties for treating acute and chronic toxoplasmosis in the mouse. Compound **24** exhibited many of the desired properties in terms of PK in the mouse. Although Cmax levels were high, it was relatively rapidly cleared from serum, likely as a consequence of metabolism in the liver as the half-life in microsomes was relatively short. This was partially offset by high oral availability and moderate protein

binding, resulting in reasonable serum profiles and good AUC profiles. However, we were only able to obtain free serum levels that exceeded the EC_{50} based on free drug for a period of ~ 2 hr after oral dosing in the mouse. Nonetheless, dosing schemes of 25-50 mg/kg were able to decrease acute infection, preventing weight loss and death in a majority of immunocompetent animals. Additionally, treatment during acute infection resulted in dramatically lower cyst counts during chronic infection, likely as a consequence of decreasing dissemination to the CNS. Indeed, treatment was sufficient to provide a complete cure in one animal with no evidence of chronic infection.

Although previous studies have largely focused on the acute infection model, the primary concern for immunocompromised patients is the reactivation of prior chronic infections [9]. Here we modeled this situation using severely immunocompromised Ifngr$^{-/-}$ mice, which are highly susceptible to *T. gondii* infection [37]. As Ifngr$^{-/-}$ mice completely lack the ability to respond to IFNγ, a critical mediator of host defense, it is likely that a single tissue cyst, or single viable organism, is capable of causing lethal infection in this model. Hence they provide an extremely sensitive measure of the ability of compounds to cure infection. Treatment with atovaquone [38] or artemisinin [41] derivatives is able to prolong survival of such severely immunocompromised mice, but treated animals ultimately always succumb to infection following removal of these drugs. Similarly, treatment with sulfadiazine is only able to prevent lethal infection in this model, but not eliminate the tissue cysts, such that when it is removed, animals quickly succumb due to reactivation of rapidly growing trachyzoites. Treatment with compound **24** prolonged survival of Ifngr$^{-/-}$ mice and resulted in a radical cure in some animals, a result not previously seen with other compounds. The efficacy of compound **24** in this model

likely stems from its ability to block tachyzoite invasion and egress, but it was also able to block bradyzoite invasion in vitro, suggesting it may directly affect the formation and turnover of cysts in vivo. Other PP analogs have been reported to reduce the chronic cyst burden in infected mice, albeit at very high serum doses, which exceed the level where they are selective for CDPK1 [19]. In contrast, compound **24** retains anti-toxoplasma activity at very modest serum levels, which are well within the range where it is selective for CPDK1 in *T. gondii* [12, 23].

CONCLUSIONS

CDPK is an essential kinase in *T. gondii* and hence has been the focus of development of potent and selective inhibitors. Here we report new PP inhibitors that were designed to improve metabolic stability and specificity for CDPK1. The optimal molecule in this series compound **24** showed low nanomolar inhibition of CDPK1 in vitro, submicromolar inhibition of parasite growth in vitro, and improved metabolic stability. In vivo administration of this analog, which showed excellent oral availability and moderate PK parameters, decreased the severity of acute infection, reduce tissue cyst levels, and delay reactivation of chronic toxoplasmosis in the mouse. Additionally, compound **24** is remarkable in being able to completely cure a portion of immunocompromised animals. As radical cure is currently not possible for humans infected with *T. gondii*, compounds that can achieve this goal with higher efficacy would greatly enhance the potential utility of PP analogs for treatment of toxoplasmosis. Collectively, these advances underscore the utility of the PP scaffold as a new therapeutic agent for treatment of acute and chronic toxoplasmosis.

EXPERIMENTAL SECTION

Chemical synthesis. Starting materials, solvents and reagents obtained commercially were reagent grade and were used without further purification. NMR spectra were obtained at the University of California, San Francisco NMR facility: ^{1}H NMR were recorded on a Bruker AvanceIII HD 400 at 400 MHz and ^{13}C spectra were recorded on a Bruker AvanceIII HD 400 at 400 MHz or a Bruker Advance DRX500. High-resolution mass spectra (HRMS) were acquired by electrospray ionization (ESI) in positive ion mode using Finnigan LTQ FT mass spectrometer (Thermo) at the QB3/Chemistry Mass Spectrometry Facility (University of California, Berkeley). Samples were directly injected into ESI source via syringe pump with flow rate 5 uL/min. Reactions were monitored by thin layer chromatography (TLC), using Merck silica gel 60 F254 glass plates (0.25 mm thick). Flash chromatography was conducted with Teledyne Isco RediSep Rf silica flash cartridges on a Teledyne Isco CombiFlash Rf+. All RP-HPLC were performed with a Waters 2545 binary gradient module equipped with an XBridge prep C18 column using H_2O + 0.1% formic acid and CH3CN + 0.1% formic acid (5-95% gradient) while monitoring at 254 nm. All final compounds were >95% pure as measured by Liquid Chromatography Mass Spectrometry (LCMS) using a Waters Acquity UPLC/ESI-TQD BEH C18 (1.7 µm) column using H_2O + 0.1% formic acid and CH3CN + 0.1% formic acid (5-95% gradient) over 1.8 min at 600 µL/min. Full compound characterization details are presented in the supporting information. All compounds reported here were screened for Pan Assay Interference (PAINS) and found to pass all the filters based contained in the FAF-Drugs4 web-server (http://fafdrugs4.mti.univ-paris-diderot.fr/).

Parasite strains and cell lines. Tachyzoites of *T. gondii* strains were grown in monolayers of human foreskin fibroblasts (HFF) maintained in complete medium (DMEM containing 10% FBS, 10 mM glutamine, and 10 μg/ml gentamycin) at 37°C in 5% CO_2. Following natural egress, tachyzoites were purified in HBSS containing 10 mM HEPES, 0.1 mM EGTA and separated from host debris using 3.0 micro polycarbonate membrane filters, followed by centrifugation at 400*g*. HFF monolayers obtained from an anonymous donor were provided by Dr. John Boothroyd's laboratory (Stanford University). All strains and host cell lines were determined to be mycoplasma negative using the e-Myco plus kit (Intron Biotechnology).

Enzyme expression and purification. Full-length *T. gondii* CDPK1 enzyme was expressed with a C-terminal His tag in pET22b(+), as described previously [12]. CDPK1 was expressed in BL21 (DE3)V2RpAcYc-LIC+LamP E coli, which contains the LamP phosphatase. A cDNA fragment encoding human Src (hSrc) kinase domain ranging from amino acids 254-536 amino acids was amplified using the primers Scr-F (GATATACATATGCAGACTCAGGGCCTGGC) and Scr-R (GTGGTGCTCGAGGAGGTTCTCCCC), and cloned into pET22b using restriction enzymes NdeI and XhoI. hSrc containing a Thr gatekeeper residue (equivalent of Thr338 in the full length sequence of the c-Src allele) was expressed in BL21 (DE3)V2RpAcYc-LIC+LamP E coli, which contains the LamP phosphatase. Following overnight growth in Terrific Broth at 37°C, the culture was diluted 1:100 and grown for 3 hr at 37°C (O.D. 0.6-0.8), then induced with 0.3 mM IPTG during overnight growth at 15°C or 30°C. Cells were lysed by sonication and soluble proteins purified using HIS-select Nickel Affinity Gel. Purified proteins were dialyzed (50 mM Tris-HCL, pH7.5, 150

mM NaCl), and stored in 25% glycerol containing 0.5 mM DTT at -80°C. Protein purity and concentrations were determined by SDS-PAGE and staining with SYPRO Ruby (Invitrogen).

Crystallography method. For the purpose of crystallization, recombinant *Tg*CDPK1 was expressed, purified, and set up in crystal trial with inhibitors as previously described [14]. Diffracting crystals were obtained by co-crystalization with compounds **3** (PDB code: 5W9E), **1** (PDB code: 5W8R), **2** (PDB code: 41H8), **13** (PDB code: 5W80), and **4** (PDB code: 5W91). Crystallographic data were collected at beam line 19ID of Argonne National Laboratory's Advanced Photon Source (http://www.sbc.anl.gov/index.html) and processed using *HKL-3000* [42]. All structures were solved using Phaser for molecular replacement and the previously deposited *Tg*CDPK1 coordinates (PDB code: 41H8) as a search model. The models were refined using *Buster* [43] and *REFMAC* [44] combined with iterative manual model building using the molecular graphics program *Coot* [45]. The geometry of all final models was checked using *MolProbity* [46]. Crystallographic details and refinement statistics are summarized in Table S1. Atomic coordinates and experimental data will be released on publication.

Homology modeling. Compound **24** was modeled using the co-crystal structure of compound **13** (PDB code: 5W9E) in Molecular Operating Environment (MOE) version 2015.1 by Chemical Computing Group [47]. Di-Fluorine was added to the piperidine of compound **13** using the ligand builder to create compound **24** and the structure was prepared and minimized using LigX with the Amber10:EHT force field (used Protonate3D for protonation, allowed ASN/GLN/HIS "Flips" in Protonate3D, deleted water molecules farther than 4.5Å from compound **24** or CDPK1, tethering parameters:

receptor strength at 5000 to minimize large changes to the CDPK1 backbone, fixed atoms father than 8Å away from compound **24**, hydrogens close to compound **24** not fixed, and refined compound **24**-CDPK complex to an RMS gradient of 0.1kcal/mol/Å).

Enzyme assays and IC_{50}s. CDPK1 activity was monitored based on phosphorylation of syntide-2 peptide (Callbiochem) that was detected using mAb MS-6E6 (MBL Intl, Corp) using an ELISA protocol described previously [23]. Kinase reactions were conducted at 30°C for 20 min in 20 mM HEPES, pH 7.5, 10 mM $MgCl_2$, 1 mM DTT, 2.5 mM $CaCl_2$, 0.1 mM EGTA, 0.005% Tween 20. Reactions were conducted using 25 μM ATP (the Km for the enzyme) using 140 ng of kinase per reaction. To determine the potency of inhibitors, duplicate wells were treated with a range of compound concentrations from 10 μM to 0.5 nM. Inhibitors were pre-incubated with the enzyme in the reaction buffer for 10 min before addition of ATP. Individual IC_{50} values were determined from two or more independent biological replicates and are reported as mean values. Src activity was monitored by phosphorylation if the Abltide peptide (EAIYAAPFAKKK, Enzo Life Sciences) that was detected using a monoclonal antibody to phosphotyrosine (Sigma) using an ELISA protocol similar to that used for CDPK1 above. Kinase reactions were conducted in 50 mM Tris-HCl, pH 7.5, 10 mM $MgCl_2$, 2.5 nM $MnCl_2$, 0.2 mM DTT, 0.5 mM EGTA. Reactions were conducted using 5 μM ATP (the Km for the enzyme) using 75 ng of kinase per reaction. Compounds were tested at 10 μM in duplicate, in two biological replicates, and values are reported as mean ± S.D. For compounds that showed > 50% inhibition at 10 μM, serial dilutions from 10 μM to 0.5 nM were tested in duplicate to derive IC_{50} values.

CK1ε (ThermoFisher) activity was monitored based on phosphorylation of dephosphorylated casein (Sigma-Aldrich) under the following conditions: 50mM TRIS (pH 7.4), 10mM $MgCl_2$, 0.4 mg/mL casein, 2.5 mM DTT, 2% DMSO, 0.1 mg/mL BSA, 2 μM ATP (Km_{app}), 1μCi 32P-ATP (Perkin Elmer), 5 nM CK1ε. Additional activity assays were done at 100 μM ATP with 10nM kinase. To determine the potency of inhibitors, duplicate wells were treated with a 10-fold dilution of compound from 200 μM to 200 pM. Inhibitors were pre-incubated with the enzyme in the reaction buffer for 15 min before addition of ATP and 32P-ATP. Upon completion of the reaction (10 minutes for Km_{app}, 55 minutes for 100 μM ATP) 3μL was spotted onto P81 paper. The paper was dried for 5 minutes under a heat lamp followed by 1x30second wash and 6x5min washes in 1% Phosphoric Acid. The paper was dried for 15 minutes under a heat lamp followed by overnight exposure to a phosphor screen imaged on a Typhoon 9500. Intensities were quantified using densitometry and IC_{50} values were determined from quantification of two independent biological replicates of triplicate dose response determined by fitting the data to a sigmoid function in Prism 7.0 (GraphPad Software) and are reported as mean values.

Kinome screen. Human kinome profiling was conducted using the ThermoFisher Scientific SelectScreen ACCESS program to profile 489 kinases utilizing three assay formats: Z'-LYTE (284 kinases), Adapta (39 kinases), and LanthaScreen (166 kinases). Z'-LYTE and Adapta yield % inhibition values based on the mean of 2 points that measure the ability of the compound to inhibit an active kinase. LanthaScreen yields % displacement values based on the mean of 2 points that measure the ability of the

inhibitor to displace a tracer bound to an inactive or weakly active kinase. Inhibitors were screened at 1 μM.

Parasite growth assays and EC_{50}s. Parasite growth inhibition assays were conducted using the type I RH strain, 2F clone that expresses bacterial β-galactosidase (β-gal), as described previously [23]. Compounds dissolved in DMSO at 10 mM stocks were diluted in medium to two times final concentrations and added to an equal volume of medium containing 5 x 10^2 parasites and incubated for 20 min. Mixtures of compounds (ranging from 10 μM to 0.01 nM) containing 0.1% (v/v) DMSO, or DMSO alone were added to monolayers of HFF cells grown in 96 well plates, centrifuged at 300 *g* for 5 min, and returned to culture at 37°C, 5% CO_2. After 4 hr, the plates were washed to remove extracellular parasites and compounds, and then returned to culture for 72 hr. At the end of the incubation period, the monolayer was lysed in 1% Triton X-100 and β-gal activity monitored using 1 mM chlorophenol red-β-D-galactopyranoside by absorption at 570 nm, as described previously [23]. Individual EC_{50} values were determined from three or more independent biological replicates and are reported as mean values.

Host toxicity assays. HFF cells were plated in complete medium and allowed to adhere for 4 hr at 37°C, 5% CO_2. Compounds diluted to 10 μM in 0.1% (v/v) DMSO, or DMSO alone, were then added and cells were incubated for an additional 72 hr. Following the incubation period, samples were evaluated using a cell proliferation assay (CellTiter 96 Aqueous Non-Radioactive Cell Proliferation Assay, Promega Corporation). As a positive control, mitomycin C (10 μM) was included in each plate. Compounds were tested in duplicate, in two biological replicates, and values are reported as means ± S.D.

In vitro analysis of uptake, efflux, metabolism, and protein binding

Assays to monitor uptake and efflux of compounds by polarized epithelial cells were conduced by Absorption Systems Inc. (Exton, PA, USA). In brief, Caco-2 cells (Clone C2BBel from ATCC) were grown to confluence on collagen-coated polycarbonate membranes on transwell plates. Permeability assays were conducted in Hank's balanced salt solution, containing 10 mM HEPES, 10 mM glucose, pH 7.4. Compounds were added at 5 μM to the apical (A) vs. basolateral (B) side and duplicate samples taken at 120 min. Samples were analyzed by LC-MS/MS and expressed as apparent permeability (P_{app}) for uptake (A to B) vs. efflux (B to A) and efflux ration (P_{app}(B to A) / P_{app}(A to B)).

The stability of compounds in the presence of rat or mouse liver microsomes was conducted by Absorption Systems, Inc. In brief, rat liver microsomes, or mouse rat liver microsome were incubated with compounds at 1 μM in a shaking water bath for 60 min. Aliquots were withdrawn at intervals, extracted, and analyzed by LC-MS/MS to evaluate the remaining parent compound. Half-lives were calculated using a single-phase exponential decay equation (Graph Pad). Intrinsic clearance was calculated as CL_{int} = k/P, where k is the elimination rate constant and P is the protein concentration in the assay. For plasma protein binding, compounds were incubated at 5 μM in CD-1 mouse plasma and protein bound fractions were monitored by equilibrium dialysis.

In vivo pharmacokinetic studies

Pharmacokinetic (PK) studies were conducted by Sai Life Sciences Limited (India). Compounds were administered orally in 50% PEG-400 in PBS, while for i.v. administration, compounds were dissolved in 20% PEG-400 -PBS. Mean plasma

concentrations were determined following a single i.v. dose of 3 mg / kg in male Swiss Albino mice by sampling at 0.05, 0.25, 1, 2, 4 and 8 hrs. Separately, male mice were used for monitoring mean plasma concentrations following single oral dose 10 /mg / kg with similar time points. Separate animals were used to determine the brain distribution relative to plasma levels at 1 hr following a single oral dose of 10 mg/ kg. Selected compounds were tested for dose response of plasma concentrations following single or multiple oral administration of a single dose of 10, 25, and 50 mg/ kg at time intervals of 0.25, 1, 2, 4, 8 and 24 hr. Plasma samples were separated processed by precipitation in acetonitrile and analyzed by LC-MS/MS. Pharmacokinetic parameters, including those for plasma versus brain, and oral bioavailability, were calculated with the non-compartmental analysis tools of the Phoenix WinNonLin (v6.3).

Animal Studies

Animals were obtained from Jackson Laboratories and housed at Washington University in accordance with the U.S.A. Public Health Service Policy on Humane Care and Use of Laboratory Animals. Animals were maintained in an Association for Assessment and Accreditation of Laboratory Animal Care approved facilities and were approved by the Institutional Animal Studies Committee at the School of Medicine, Washington University in St. Louis.

Ex vivo bradyzoite treatment assays. Adult (8-12 weeks old) female CD1 mice were infected with tachyzoites of the PruΔ*hxg*Δ*ku8*0; LDH2-GFP (PRU-GFP) [48] or ME49Δ*hx*::FLUC [49] strains expressing firefly luciferase (FLUC) [49] and allowed to develop chronic infections. Adult (8-12 weeks old) CBA/J mice were orally infected with 10-20 tissue cysts of the ME49Δ*hx*::FLUC strain. At 3-6 weeks post-inoculum, brains

were isolated from 2-3 animals and tissue cysts purified from brain homogenate by Percoll gradient, as previously described [11]. A serological pipette was used to isolate the ~9.0 mL of gradient between the erythrocyte layer and the brain homogenate layer after the initial centrifugation step (1,200*g* for 15 min at 4°C). Following purification, cysts were resuspended in acid-pepsin solution (170 mM NaCl, 60 mM HCl, 0.1 mg/mL pepsin (1:10,000 activity)), incubated for 10 min at 37°C and then neutralized by addition of sodium carbonate solution (94 mM). Liberated bradyzoites were inoculated into parallel 6-well plates containing HFF monolayers with compounds (constant treatment vs. washout). At 4 hr post-infection, the washout 6-well plate was rinsed 3 times in fresh media to remove cell debris and non-invaded parasite and returned to incubator with fresh culture medium lacking compound. The constant treatment plate was allowed to incubate without washing. Plates were incubated for 10-14 days prior to ethanol fixation, staining with 0.1% crystal violet stain, and plaques counted using an Axio Observer.D1 microscope under 2.5x magnification.

Treatment during acute challenge studies

Adult (8-12 weeks old) female Balb/C mice were infected with 5,000 tachyzoites of the type II ME49Δ*hx*::FLUC line by i.p. injection. At 24 hr post-infection animals were dosed with compounds formulated in 25% PEG-PBS containing 5% DMSO, or 25% PEG-400-PBS- 5% DMSO alone, by oral gavage and treatment was continued for 6 days. Treated mice received one day 1, an initial loading dose of compound **24** at 50 mg/kg in the morning, followed twelve hr later by a second dose of 25 mg/kg, and then 25 mg/kg BID for 5 additional days. Bioluminescence imaging (see below) was used to monitor infection from day 6 to 20, and weight loss and survival were tracked over the first 30

days. At the end of 30 days, tissue cysts in the brain were quantified by staining with *Dolichos biflorus* lectin that was labeled with FITC, and microscopic examination, as described previously [50]. For samples were no cysts were observed (lower threshold = 40 per brain), residual infection was tested by bioassay into a naïve recipient. For bioassay experiments, 200 μL of brain homogenate was injected i.p. into a recipient Ifngr1$^{-/-}$ mouse, which lack the ability to control parasite proliferation and readily succumb to infection [37].

Treatment during reactivation of chronic toxoplasmosis

To provide a model for treatment during reactivation of chronic infection, we used a modification of a previously published protocol [38, 41]. Male and female Ifngr1$^{-/-}$ mice were orally infected with 5 cysts of the type II ME49Δ*hx*::FLUC line, obtained from the brains of chronically infected wild type CD-1 mice. Animals were treated with sulfadiazine (0.25 g/L in the drinking water) from day 2-22. Two days (48 hr) after removal of the sulfadiazine, compound **24** formulated in 25% PEG-400-PBS containing 5% DMSO, or 25% PEG-400-PBS- 5% DMSO alone (control), were administered by oral gavage for a total of 8 days. One group of treated mice received one day 1, an initial loading dose of compound **24** at 50 mg/kg in the morning, followed twelve hr later by a second dose of 25 mg/kg, and then 25 mg/kg BID for 7 additional days. A second group of animals received compound **24 at** 40 mg/kg BID for 8 days. Animals were monitored for weight loss, bioluminescence imaging, and survival for 30 days. At the end of 30 days, animals were examined for presence of cysts in the brain and by bioassay by inoculation of brain homogenate (200 μL of 1 ml) into a naïve recipient Ifngr1$^{-/-}$ mouse, as described above. There were no differences in outcome associated with the sex of animals.

Bioluminescence imaging

Animals were monitored for bioluminescence using a Xenogen IVIS200 instrument and analyzed using the Xenogen Living Image software (Caliper Life Sciences). Mice were anesthetized using 2% isoflurane and injected i.p. with D-luciferin (Biosynth AG) at 150 mg/ mg just prior to imaging.

Statistical analyses. Mathematical and statistical analyses were conducted in Prism (GraphPad). IC_{50} and EC_{50} values were determined using normalized, log-transformed (conc.) data fit with nonlinear regression analysis based on sigmoidal dose-response curves with variable slope. For correlating IC_{50} to EC_{50} values, r^2 values were generated using linear regression analysis. Mean values for inhibition of bradyzoite plaque formation were analyzed using two-way ANOVA with Dunnett's correction for multiple comparisons. Survival curves were plotted as Kaplan Meier survival curves and significance determined by the Mantel-Cox test. Mean values for bioluminescence and weight loss were compared using Student's t-test with Holm-Sidak correction for multiple tests. The average numbers of cysts per brain where compared using a Mann-Whitney non-parametric test for non-normally distributed data with unequal variance. For all test, a minimum value of $P \leq 0.05$ was considered significant and individual values are given in the figure legends.

Ancillary Information

Supporting information:

Compound synthesis, characterization, metabolism analysis, x-ray crystallography information, kinome profiling (**PDF**)

Molecular Formula Strings (**CSV**)

Compound 24 Homology Model (**PDB**)

PDB ID Codes: The structure factors and pdb coordinates have been deposited at the protein databank (PDB) with the coordinates 4IHP, 5W8R, 5W80, 5W9E, and 5W91. Authors will release the atomic coordinates and experimental data upon article publication.

Homology models: Compound **24** was modeled using the co-crystal structure of compound **13** (PDB code: 5W9E). Authors will release the atomic coordinates and experimental data upon article publication.

Corresponding Author Information: Email: sibley@wustl.edu, Phone 314-362-8873, ORCID: Oid4lds1

Author contributions: Florentine Rutaganira and Michael S. Lopez performed the chemical syntheses and physical characterization of the compounds described here. Jennifer Barks performed the in vitro cell-based assays for parasite and host cell growth inhibition. Mary Savari Dhason and Shaojun Long performed the enzyme purification and enzyme assays. Qiuling Wang conducted the animal studies with assistance from L. David Sibley. Nathaniel Jones and Joshua B. Radke performed the ex vivo tissue cysts experiments. Amarendar R. Madirala purified select chemicals for in vivo studies. Jim Janetka, provide advice on chemical synthesis. Majida El Bakkouri and Ray Hui

performed the structural studies. L. David Sibley and Kevan Shokat supervised the research. Florentine Rutaganira and L. David Sibley performed data analyses, generated the figures, and wrote the manuscript with input from all authors.

Acknowledgement: We are grateful to Keliang Tang who performed the initial studies on enzyme kinetics and established the enzyme assays and to Martin John Rodgers for his early support of this project. We also thank John R. Walker of the Structural Genomics Consortium for verifying the crystallographic structures and for their deposition into the Protein Data Bank and the UCSF NMR Lab and QB3/Chemistry Mass Spectrometry Facility (University of California, Berkeley) for access to instrumentation for compound characterization. Supported by a grant from the NIH (AI094098 to K.M.S. and L.D.S.). The compounds reported here are the subject of patent applications filed by UCSF and Washington University.

Abbreviations Used: □□□□□□□□□□□□□□□□□□□□□□□□□□□□□□□□ β-gal, β-galactosidase; BID, bis in die (twice a day); CDPK1, calcium dependent protein kinase 1; CNS, central nervous system; EC_{50}, 50% effective concentration; ELISA, enzyme-linked immunosorbent assay; HAART, highly active anti-retroviral therapy; HFF, human foreskin fibroblast; HIV, human immunodeficiency virus; IC_{50}, 50% inhibitor concentration; FLUC, firefly luciferase; SAR, structure activity relationship;

References

1. Montoya, J. G.; Liesenfeld, O. Toxoplasmosis. *Lancet* **2004,** 363, 1965-1976.
2. Dennis, A. M.; Napravnik, S.; Sena, A. C.; Eron, J. J. Late entry to HIV care among Latinos compared with non-Latinos in a southeastern US cohort. *Clin. Infect. Dis.* **2011,** *53*, 480-487.
3. Kiderlen, T. R.; Liesenfeld, O.; Schurmann, D.; Schneider, T. Toxoplasmic encephalitis in AIDS-patients before and after the introduction of highly active antiretroviral therapy (HAART). *Eur. J. Clin. Microbiol. Infect. Dis.* **2011,** *30*, 1521-1525.
4. Oliveira, J. F.; Greco, D. B.; Oliveira, G. C.; Christo, P. P.; Guimaraes, M. D.; Oliveira, R. C. Neurological disease in HIV-infected patients in the era of highly active antiretroviral treatment: a Brazilian experience. *Rev. Soc. Bras. Med. Trop.* **2006,** *39*, 146-151.
5. Palella, F. J.; Delaney, K. M.; Moorman, A. C.; Loveless, M. O.; Fuhrer, J.; Satten, G. A.; Aschman, D. J.; Holmberg, S. D.; The HIV Outpatient Study Investigators. Declining morbidity and mortality among patients with advanced human immunodeficiency virus infection. *N. Engl. J. Med.* **1998,** *13*, 853-860.
6. Israelski, D. M.; Remington, J. S. Toxoplasmosis in the non-AIDS immunocompromised host. *Curr. Clin. Top. Infect. Dis.* **1993,** *13*, 322-356.
7. Arantes, T. E.; Silveira, C.; Holland, G. N.; Muccioli, C.; Yu, F.; Jones, J. L.; Goldhardt, R.; Lewis, K. G.; Belfort, R., Jr. Ocular involvement following postnatally acquired

Toxoplasma gondii infection in southern Brazil: A 28-year experience. *Am. J. Ophthalmol.* **2015,** *159*, 1002-1012 e1002.

8. Jacobson, J. M.; Davidian, M.; Rainey, P. M.; Hafner, R.; Raasch, R. H.; Luft, B. J. Pyrimethamine pharmacokinetics in human immunodeficiency virus-positive patients seropositive for *Toxoplasma gondii*. *Antimicrob. Agents Chemother.* **1996,** *40*, 1360-1365.
9. McCabe, R. E. Antitoxoplasma chemotherapy. In *Toxoplasmosis: a Comprehensive Clinical Guide*, Joynson, D. H. M.; Wreghitt, T. G., Eds. Cambridge Univ. Press: Cambridge, 2001; pp 319-359.
10. Weiss, L. M.; Kim, K. Bradyzoite development. In *Toxoplasma gondii the Model Apicomplexan: Perspectives and Methods*, Weiss, L. M.; Kim, K., Eds. Academic Press: New York, 2007; pp 341-366.
11. Watts, E.; Zhao, Y.; Dhara, A.; Eller, B.; Patwardhan, A.; Sinai, A. P. Novel approaches reveal that *Toxoplasma gondii* bradyzoites within tissue cysts are dynamic and replicating entities in vivo. *MBio* **2015,** *6*, e01155-01115.
12. Lourido, S.; Shuman, J.; Zhang, C.; Shokat, K. M.; Hui, R.; Sibley, L. D. Calcium-dependent protein kinase 1 is an essential regulator of exocytosis in Toxoplasma. *Nature* **2010,** *465*, 359-362.
13. Ojo, K. K.; Larson, E. T.; Keyloun, K. R.; Castaneda, L. J.; DeRoucher, A. E.; KInampudi, K. K.; Kim, J. E.; Arakaki, T. L.; Murphy, R. C.; Zhang, L.; Napuli, A. J.; Maly, D. J.; Verlinde, C. L. M. J.; Buckner, F. S.; Parsons, M.; Hol, W. G. J.; Meritt, E. A.; Van Voorhis, C. *Toxoplasma gondii* calcium-dependent protein kinase 1 is a target for selective kinase inhibitors. *Nat. Struct. Molec. Biol.* **2010,** *17*, 602-607.

14. Wernimont, A. K.; Artz, J. D.; Finerty, P.; Lin, Y.; Amani, M.; Allali-Hassani, A.; senisterra, G.; Vedadi, M.; Tempel, W.; Mackenzie, F.; Chau, I.; Lourido, S.; Sibley, L. D.; Hui, R. Structures of apicomplexan calcium-dependent protein kinases reveal mechanism of activation by calcium. *Nat. Struct. Molec. Biol.* **2010,** *17*, 596-601.

15. Manning, G.; Whyte, D. B.; Martinez, R.; Hunter, T.; Sudarsanam, S. The protein kinase complement of the human genome. *Science* **2002,** *298*, 1912-1934.

16. Hui, R.; El Bakkouri, M.; Sibley, L. D. Designing selective inhibitors for calcium-dependent protein kinases in apicomplexans. *Trends Pharmacol. Sci.* **2015,** *36*, 452-460.

17. Bishop, A. C.; Shah, K.; Liu, Y.; Witucki, L.; Kung, C.; Shokat, K. M. Design of allele-specific inhibitors to probe protein kinase signaling. *Curr. Biol.* **1998,** *8*, 257-266.

18. Liu, Y.; Bishop, A.; Witucki, L.; Kraybill, B.; Shimizu, E.; Tsien, J.; Ubersax, J.; Blethrow, J.; Morgan, D. O.; Shokat, K. M. Structural basis for selective inhibition of Src family kinases by PP1. *Chem. Biol.* **1999,** *6*, 671-678.

19. Johnson, S. M.; Murphy, R. C.; Geiger, J. A.; DeRocher, A. E.; Zhang, Z.; Ojo, K. K.; Larson, E. T.; Perera, B. G.; Dale, E. J.; He, P.; Reid, M. C.; Fox, A. M.; Mueller, N. R.; Merritt, E. A.; Fan, E.; Parsons, M.; Van Voorhis, W. C.; Maly, D. J. Development of *Toxoplasma gondii* calcium-dependent protein kinase 1 (TgCDPK1) inhibitors with potent anti-toxoplasma activity. *J. Med. Chem.* **2012,** *55*, 2416-2426.

20. Larson, E. T.; Ojo, K. K.; Murphy, R. C.; Johnson, S. M.; Zhang, Z.; Kim, J. E.; Leibly, D. J.; Fox, A. M.; Reid, M. C.; Dale, E. J.; Perera, B. G.; Kim, J.; Hewitt, S. N.; Hol, W. G.; Verlinde, C. L.; Fan, E.; Van Voorhis, W. C.; Maly, D. J.; Merritt, E. A. Multiple

determinants for selective inhibition of apicomplexan calcium-dependent protein kinase CDPK1. *J. Med. Chem.* **2012,** *55*, 2803-2810.

21. Murphy, R. C.; Ojo, K. K.; Larson, E. T.; Castellanos-Gonzalez, A.; Perera, B. G.; Keyloun, K. R.; Kim, J. E.; Bhandari, J. G.; Muller, N. R.; Verlinde, C. L.; White, A. C.; Merritt, E. A.; Van Voorhis, W. C.; Maly, D. J. Discovery of potent and selective inhibitors of calcium-dependent protein kinase 1 (CDPK1) from *C.ryptosporidium parvum* and *Toxoplasma gondii*. *ACS Med. Chem. Lett.* **2010,** *1*, 331-335.

22. Doggett, J. S.; Ojo, K. K.; Fan, E.; Maly, D. J.; Van Voorhis, W. C. Bumped kinase inhibitor 1294 treats established *Toxoplasma gondii* infection. *Antimicrob. Agents Chemother.* **2014,** *58*, 3547-3549.

23. Lourido, S.; Zhang, C.; Lopez, M. S.; Tang, K.; Barks, J.; Wang, Q.; Wildman, S. A.; Shokat, K. M.; Sibley, L. D. Optimizing small molecule inhibitors of calcium-dependent protein kinase 1 to prevent infection by *Toxoplasma gondii*. *J. Med. Chem.* **2013,** *56*, 3068-3077.

24. Vidadala, R. S.; Rivas, K. L.; Ojo, K. K.; Hulverson, M. A.; Zambriski, J. A.; Bruzual, I.; Schultz, T. L.; Huang, W.; Zhang, Z.; Scheele, S.; DeRocher, A. E.; Choi, R.; Barrett, L. K.; Siddaramaiah, L. K.; Hol, W. G.; Fan, E.; Merritt, E. A.; Parsons, M.; Freiberg, G.; Marsh, K.; Kempf, D. J.; Carruthers, V. B.; Isoherranen, N.; Doggett, J. S.; Van Voorhis, W. C.; Maly, D. J. Development of an orally available and central nervous system (CNS) renetrant *Toxoplasma gondii* calcium-dependent protein kinase 1 (TgCDPK1) inhibitor with minimal human ether-a-go-go-related gene (hERG) activity for the treatment of toxoplasmosis. *J. Med. Chem.* **2016,** *59*, 6531-6546.

25. Hanefeld, U.; Rees, C. W.; White, A. J. P.; Williams, D. J. One-pot synthesis of tetrasubstituted pyrazoles - proof of regiochemistry. *J. Am. Chem. Soc.* **1996,** *0*, 1545-1552.

26. Schenone, S.; Radi, M.; Musumeci, F.; Brullo, C.; Botta, M. Biologically driven synthesis of pyrazolo[3,4-d]pyrimidines as protein kinase inhibitors: an old scaffold as a new tool for medicinal chemistry and chemical biology studies. *Chem. Rev.* **2014,** *114*, 7189-7238.

27. Kwong, F. Y.; Buchwald, S. L. A general, efficient, and inexpensive catalyst system for the coupling of aryl iodides and thiols. *Org. Lett.* **2002,** *4*, 3517-3520.

28. Ley, S. V.; Thomas, A. W. Modern synthetic methods for copper-mediated C(aryl)-O, C(aryl)-N, and C(aryl)-S bond formation. *Angewandte Chem.* **2003,** *42*, 5400-5449.

29. Ma, D.; Cai, Q. N,N-dimethyl glycine-promoted ullmann coupling reaction of phenols and aryl halides. *Org. Lett.* **2003,** *5*, 3799-3802.

30. Prim, D.; Campagne, J.-m.; Andrioletti, B. Palladium-catalysed reactions of aryl halides with soft, non-organometallic nucleophiles. *Tetrahedron* **2002,** *58*, 2041-2075.

31. Zaretzki, J.; Matlock, M.; Swamidass, S. J. XenoSite: accurately predicting CYP-mediated sites of metabolism with neural networks. *J. Chem. Inform. Model.* **2013,** *53*, 3373-3383.

32. Bohm, H. J.; Banner, D.; Bendels, S.; Kansy, M.; Kuhn, B.; Muller, K.; Obst-Sander, U.; Stahl, M. Fluorine in medicinal chemistry. *Chembiochem* **2004,** *5*, 637-643.

33. Barnes-Seeman, D.; Jain, M.; Bell, L.; Ferreira, S.; Cohen, S.; Chen, X. H.; Amin, J.; Snodgrass, B.; Hatsis, P. Metabolically stable tert-butyl replacement. *ACS Med. Chem. Lett.* **2013,** *4*, 514-516.

34. Hicken, E. J.; Marmsater, F. P.; Munson, M. C.; Schlachter, S. T.; Robinson, J. E.; Allen, S.; Burgess, L. E.; Delisle, R. K.; Rizzi, J. P.; Topalov, G. T.; Zhao, Q.; Hicks, J. M.; Kallan, N. C.; Tarlton, E.; Allen, A.; Callejo, M.; Cox, A.; Rana, S.; Klopfenstein, N.; Woessner, R.; Lyssikatos, J. P. Discovery of a novel class of imidazo[1,2□a]pyridines with potent PDGFR activity and oral bioavailability. *ACS Med. Chem. Lett.* **2014,** *5*, 78-83.

35. Shim, H. J.; Kim, H. I.; Lee, S. T. The associated pyrazolopyrimidines PP1 and PP2 inhibit protein tyrosine kinase 6 activity and suppress breast cancer cell proliferation. *Oncol. Lett.* **2017,** *13*, 1463-1469.

36. Lourido, S.; Jeschke, G. R.; Turk, B. E.; Sibley, L. D. Exploiting the unique ATP-binding pocket of toxoplasma calcium-dependent protein kinase 1 to identify its substrates. *ACS Chem. Biol.* **2013,** *8*, 1155-1162.

37. Yap, G. S.; Sher, A. Effector cells of both nonhemopoietic and hemopoietic origin are required for interferon (IFN)-gamma- and tumor necrosis factor (TNF)-alpha-dependent host resistance to the intracellular pathogen, *Toxoplasma gondii*. *J. Exp. Med.* **1999,** *189*, 1083-1091.

38. Dunay, I. R.; Heimesaat, M. M.; Bushrab, F. N.; Muller, R. H.; Stocker, H.; Arasteh, K.; Kurowski, M.; Fitzner, R.; Borner, K.; Liesenfeld, O. Atovaquone maintenance therapy prevents reactivation of toxopasmic encepahalitis in the murine model of reactivated toxoplasmosis. *Antimicrob. Agents Chem.* **2004,** *48*, 4848-4854.

39. Zhang, C.; Lopez, M. S.; Dar, A. C.; Ladow, E.; Finkbeiner, S.; Yun, C. H.; Eck, M. J.; Shokat, K. M. Structure-guided inhibitor design expands the scope of analog-sensitive kinase technology. *ACS Chem. Biol.* **2013,** *8*, 1931-1938.

40. Long, A. M.; Zhao, H.; Huang, X. Structural basis for the potent and selective inhibition of casein kinase 1 epsilon. *J. Med. Chem.* **2012,** *55*, 10307-10311.

41. Dunay, I. R.; Chan, W. C.; Haynes, R. K.; Sibley, L. D. Artemisone and artemiside control acute and reactivated toxoplasmosis in the murine model. *Antimicrob. Agents Chemother.* **2009,** *53*, 4450 - 4456.

42. Minor, W.; Cymborowski, M.; Otwinowski, Z.; Chruszcz, M. HKL-3000: the integration of data reduction and structure solution--from diffraction images to an initial model in minutes. *Acta Crystallogr. D Biol. Crystallogr.* **2006,** *62*, 859-866.

43. Bricogne, G.; Blanc, E.; Brandl, M.; Flensburg, C.; Keller, P.; W., P.; Roversi, P.; Sharff, A.; Smart, O. S.; Vonrhein, C.; Womack, T. O. BUSTER version 2.10.0. *Cambridge, United Kingdom: Global Phasing Ltd.* **2011**.

44. Murshudov, G. N.; Vagin, A. A.; Dodson, E. J. Refinement of macromolecular structures by the maximum-likelihood method. *Acta Crystallogr. D Biol. Crystallogr.* **1997,** *53*, 240-255.

45. Emsley, P.; Cowtan, K. Coot: model-building tools for molecular graphics. *Acta Crystallogr. D Biol. Crystallogr.* **2004,** *60*, 2126-2132.

46. Davis, I. W.; Leaver-Fay, A.; Chen, V. B.; Block, J. N.; Kapral, G. J.; Wang, X.; Murray, L. W.; Arendall, W. B., 3rd; Snoeyink, J.; Richardson, J. S.; Richardson, D. C. MolProbity: all-atom contacts and structure validation for proteins and nucleic acids. *Nucleic Acids Res.* **2007,** *35*, W375-383.

47. Molecular Operating Environment (MOE), 2013.08. In Chemical Computing Group ULC: Montreal, QC, Canada, 2017.

48. Fox, B. A.; Falla, A.; Rommereim, L. M.; Tomita, T.; Gigley, J. P.; Mercier, C.; Cesbron-Delauw, M. F.; Weiss, L. M.; Bzik, D. J. Type II *Toxoplasma gondii* KU80 knockout strains enable functional analysis of genes required for cyst development and latent infection. *Eukaryot. Cell* **2011,** *10*, 1193-1206.

49. Tobin, C. M.; Knoll, L. J. A patatin-like protein protects Toxoplasma gondii from degradation in a nitric oxide-dependent manner. *Infect. Immun.* **2012,** *80*, 55-61.

50. Wang, Z. T.; Harmon, S.; O'Malley, K. L.; Sibley, L. D. Reassessment of the role of aromatic amino acid hydroxylases and the effect of infection by *Toxoplasma gondii* on host dopamine. *Infect. Immun.* **2015,** *83*, 1039-1047.

51. Eid, S.; Turk, S.; Volkamer, A.; Rippmann, F.; Fulle, S. KinMap: a web-based tool for interactive navigation through human kinome data. *BMC Bioinform.* **2017,** *18*, 16.

Table 1 Physical parameters, metabolic stability, efflux, and toxicity of select compounds

Cmpd	ClogP[1]	tPSA	pKa	Protein binding	Papp 10^{-6} cs/s A to B[2]	Papp 10^{-6} cs/s B to A[3]	Efflux ratio[4]	Microsomes CL_{int}[4] mL / min/mg	Cell toxicity[6]
1	3.15	66.34	-	99.2%	42.9	28.7	0.7	0.452	>10 μM
2	3.48	75.57	-	99.8%	34.8	30.6	0.9	0.281	>10 μM
10	3.41	75.57	-	98.4%	15.0	14.6	1.0	1.240	>10 μM
13	2.57	87.6	10.4	73.5%	1.07	9.58	8.9	0.019	>10 μM
24	3.0	87.6	7.1	88.3%	22.8	21.2	0.9	0.694	>10 μM
18	3.25	78.37	10.4	87.5%	2.76	25.6	9	0.072	>10 μM
28	3.57	78.37	7.1	91.8%	27.1	25.3	.9	0.887	>10 μM

[1] Determined in Chemdraw Ultra 12.0, PerkinElmer Informatics
Apparent permeability (Papp), apical to basolateral (A-B)
[2] Apparent permeability (Papp) basolateral to apical (B-A)
[3] Papp (B to A) / Papp (A to B)

[4] Cl_{lint} = k/P, where k is the elimination rate constant and P is the protein concentration in the assay

[5] Mouse liver microsomes

[6] Inhibition of replication of human HFF cells

Table 2 In vivo pharmacokinetic properties based on plasma levels of select compounds

Cmpd	Route	Dose mg/kg	Tmax hr	Co/Cmax[1] ng/ml	AUC[last] ng/ml hr	AUC[inf] ng/ml hr	T½ hr	CL[2] ml/min/kg	Vss[3] L/kg	%F[4]
1	iv	3	-	6892.94	1075.29	1081.76	2.06	46.22	1.09	-
	po	10	0.25	585.42	918.80	930.88	-	-	-	26
2	iv	3	-	5471.09	1146.49	1149.99	1.56	43.48	1.10	-
	po	10	0.25	1136.36	1172.75	1279.20	-	-	-	31
10	iv	3	-	2741.80	619.33	625.04	1.74	80	2.32	-
	po	10	0.25	76.69	85.47	91.42	-	-	-	4
13	iv	3	-	535.79	449.57	523.99	3.68	95.42	19.59	-
	po	10	2.00	182.56	757.85	891.24	-	-	-	51

24	iv	3	-	1205.19	975.90	988.58	1.56	50.58	3.68	-
	po	10	0.25	1048.80	3058.44	3547.95	-	-	-	94

[1] Cmax for po route, Co (initial conc.)

[2] CL, clearance

[3] Vss steady-state volume of distribution

[4] Oral availability determined from AUC_{last}

FIGURE LEGENDS

Scheme 1[a]

[a](i) R_1OH, copper iodide, N,N-dimethylglycine, Cs_2CO_3, dioxane, 120°C, 18 h; (ii) R_1NH_2, BrettPhosPd G3, KOtBu, dioxane, 90°C, 18h; (iii) R_1SH, copper iodide, ethylene glycol, 2-propanol, K_2CO_3, 130°C, 1 h. Positions on the PP scaffold are labeled numerically in blue italics.

Figure 1 Structure-Activity Profile of Initial CDPK1 Inhibitor Series. (A) Structures of initial CDPK1 inhibitors highlighting modifications at R_1 and heteroatom linkages of R_1 to the pyrazolopyrimidine core are shown in tabular form with associated biochemical inhibition (IC_{50}) of CDPK1, inhibition of parasite growth (EC_{50}), off-target biochemical inhibition (IC_{50}) of Src, metabolic stability in rat microsomes (half-life in minutes), and calculated clogP values. IC_{50} and EC_{50} values are the average of 2 or more biological replicates. (B) Compound **1** binds within the CDPK1 active site forming hydrogen bonds (black dashes) to the CDPK1 hinge and extends its R_1 substituent into the CDPK1 hydrophobic pocket. Amino acids in close proximity to 3CLBPP1 are labeled as well as the glycine gatekeeper (green). The orange map shows the $2F_0$-F_c simulated annealing map of compound **1** contoured at 1σ. (C) An overlay of compounds **1, 2, 3,** and **4** shows similar binding poses for inhibitors possessing heteroatom linkages.

Figure 2 Exploration of R_2 with Ether Linked Substituent. (A) Structures of CDPK1 inhibitors highlighting modifications at R_2 with *-meta* chloro and ether linkage to the pyrazolopyrimidine core are shown in tabular form with associated biochemical

inhibition (IC_{50}) of CDPK1, inhibition of parasite growth (EC_{50}), off-target biochemical inhibition (IC_{50}) of Src, metabolic stability in rat microsomes (half-life in minutes), and calculated clogP values. IC_{50} and EC_{50} values are the average of 2 or more biological replicates. (B) Compound **13** binds within the CDPK1 active site maintaining hinge binding to the CDPK1 hinge and forms an additional hydrogen bond with E135 within the CDPK1 ribose binding region.

Figure 3 Exploration of Methyl Piperidine at R_2 for Enhanced Metabolic Stability. (A) Structures of CDPK1 inhibitors highlighting modifications at R_1 with methyl piperidine at R_2 of a pyrazolopyrimidine core are shown in the top section, while modification of one compound to contain a pyrrolopyrimidine core is shown between the dotted lines. Structures of CDPK1 inhibitors highlighting modifications at R_2 on a pyrazolopyrimidine core that were generated in attempts to reduce cellular efflux are shown in the bottom section of the table. Biochemical inhibition (IC_{50}) of CDPK1, inhibition of parasite growth (EC_{50}), off-target biochemical inhibition (IC_{50}) of Src, metabolic stability in rat microsomes (half-life in minutes), and calculated clogP values. IC_{50} and EC_{50} values are the average of of 2 or more biological replicates assays. (B) Homology model of compound **24** based on the co-crystal structure of compound **13** and CDPK1.

Figure 4 Activity of PP analogs against tachyzoite and bradyzoites, and PK studies in mice. (A) Comparison of enzyme inhibition vs. parasite growth inhibition by PP analogs. Values for IC_{50} for inhibition of CDPK1 enzyme activity were plotted vs. EC_{50} values for inhibition of parasite growth. The plot was analyzed by linear regression

(solid line), shown with 95% confidence interval (dotted lines), r^2 = 0.58. Highlighted are potent inhibitors that were further profiled in the following studies. (B) Ex vivo treatment of bradyzoites with PP analogs. Top: Schematic for isolation of tissue cysts containing bradyzoites, shown for PRU-GFP strain. Following Percoll enrichment of mouse-brain derived cysts, bradyzoites were liberated by acid-pepsin treatment, followed by neutralization. Liberated bradyzoites were used to infect HFF monolayers. Compounds were used to treat parallel cultures either with continuous treatment, or following 4 hr treatment and washing to remove extracellular parasites and compounds. Bottom: Following isolation of bradyzoites from the ME49Δ*hx*::FLUC line, compounds were used to treat cultures as described in top panel. Plaque forming units were enumerated in triplicate from three independent experiments. Compounds **1**, **13** and **24** were used at 2.5 μM, while pyrimethamine (Pyr) was used at 3 μM. Mean ± S.E.M., n= 3 independent biological replicates with three technical replicates each. Two-way ANOVA with Dunnett's correction, * $P \leq 0.05$; ** $P \leq 0.01$, *** $P \leq 0.001$. (C) Pharmacokinetic analysis of compound FUR7-27 in mice. Dose dependent kinetics of serum levels of compound following oral administration. Compound **24** was suspended in 25%-PEG-400-PBS with 5% DMSO was administered by oral gavage. n=3 animals per time point. Reference lines shows the free serum level of compound **24** that would correspond to the EC_{50}.

Figure 5 Human Kinome Profiling of compounds to determine inhibitor selectivity. Selectivity of compounds towards a panel of kinases in the ThermoFisher ACCESS program that are inhibited (red) by more than 50% or show greater than 50% tracer

displacement (blue). Circle size reflects percent inhibition or displacement in the presence of inhibitor and percentages are the mean of 2 data points. % inhibition value for Src is shown as a yellow triangle and is emphasized by a dashed line connecting an * to the yellow triangle. Kinome tree images were generated using KinMap [51] and the kinase tree illustration is reproduced courtesy of Cell Signaling Technology, Inc. (www.cellsignal.com). Inhibitors were screened at 1 μM.

Figure 6 In vivo treatment of acute toxoplasmosis with compound 24. (A) Survival curve of mice infected with ME49-FLUC strain parasites and treated with compound **24** (Treated) vs vehicle control (Control) as monitored for 30 days. Animals were infected with 5,000 tachyzoites by i.p. injection on day 0. At 24 hr post-infection, animals were given compound **24** at 50 mg/kg, or vehicle control, followed by a second dose of 25 mg / kg 12 hr later and then treated with 25 mg/kg BID for 5 additional days. Mantel-Cox test, $P \leq 0.05$. (B) Weight loss of infected animals shown in A. Values are reported as % Control, which refers to the average weight at day 0 for each group treated separately. (C) Bioluminescence imaging of parasite numbers in animals shown in A. Whole body imaging was used to determine the mean intensity of luciferase signal that is expressed as relative light units (RLU). Individual animals shown by symbols, median values graphed in the lines. Student's t-test with Holm-Sidak correction for multiple tests, ***, $P \leq 0.001$. (D) The number of cysts in surviving animals from A were determined by counting aliquots of brain homogenate. Means ± S.D., n=6-9. Threshold for detection = 40 cysts. Red triangle denotes animal where bioassay was negative indicating it was cured. Mann-Whitney non-parametric test, **, $P \leq 0.01$. (E)

Bioluminescence imaging of representative control and treated mice from A imaged at day 8. (F) Bioluminescence imaging of control and treated mice from A imaged at day 18.

Figure 7 In vivo treatment of reactivation of CNS toxoplasmosis. (A) Schematic for treatment during reactivation in an immunocompromised mouse. Ifngr1$^{-/-}$ mice were infected with 10 cysts of the ME49-FLUC strain and treated from day 2-22 with sulfadiazine in the drinking water. Two days (48 hr) after removal of sulfadiazine, animals were treated p.o. with compound **24** or vehicle control (Control, n = 6) for 8 days. Animals in one group (n = 9) received a loading dose of 50 mg/kg followed by 25 mg/kg 12 hr later and then 25 mg/kg BID for seven additional days. A second group of animals (n = 5) received 40 mg/kg BID for 8 days. (B) Animals were evaluated for survival and imaged for bioluminescence over a period of 30 days. Treated mice survived significantly longer than controls, log-rank, Mantel-Cox test, $P < 0.001$ (***). Animals that survived in the treated groups (red triangles) were negative by bioassay, indicating they were cured. (C) Bioluminescence imaging at day 6 indicates that a number of control animals that have perished (red X) and remaining animals show a positive signal in the head and upper thorax. In contrast, all treated mice were alive and mice treated with 25 mg/kg show reduced signals while those treated with 40 mg/kg showed no sign of activation. Animals marked * were determined to be cured based on bioassay at the end of the experiment.

Table of Contents Graphic

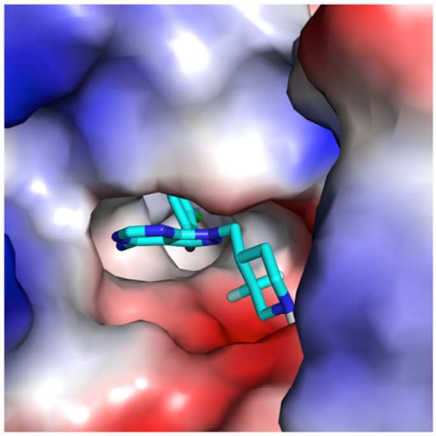

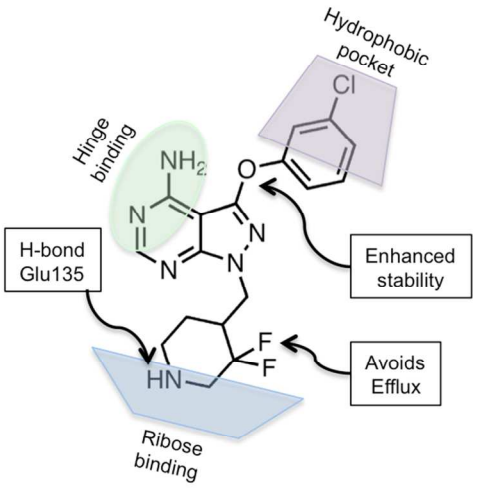

Parameter	Value
IC_{50}	10.9 nM
EC_{50}	264 nM
Src IC_{50}	> 10 mM
LogP	3.0
$T_{1/2mouse}$	1.56 hr
%F	94
Protein bound	88%
CNS/serum	1.3

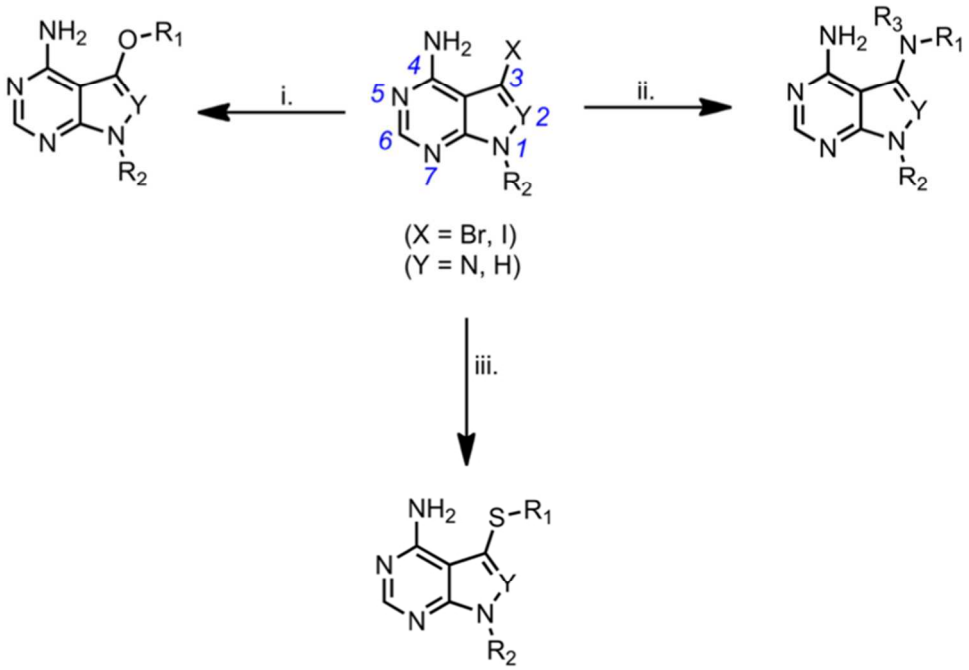

Scheme 1

83x58mm (300 x 300 DPI)

A

Compound #	R_1	CDPK1 IC_{50} (nM)	Parasite EC_{50} (nM)	Src IC_{50} (nM)	Microsome Half-Life (min)	clogP
1		3.38	167	607	4	3.31
2		9.99	497	>10,000	15.7	3.57
3		13.79	1131	>10,000	2.4	4.00
4		10.32	190	828	19.6	3.96
5		31.86	613	>10,000	10.6	2.89
6		46.98	1897	>10,000	33	3.15
7		35.12	537	>10,000	16.8	3.74
8		7.49	246	>10,000	6.2	3.72
9		8.94	305	>10,000	2.7	2.78
10		13.56	163	>10,000	4.2	3.36

B

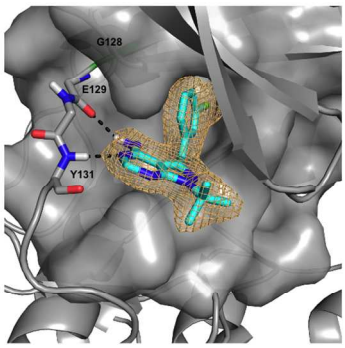

C

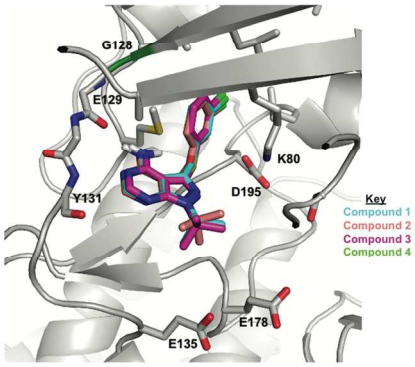

Figure 1

177x133mm (300 x 300 DPI)

A

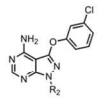

Compound #	R_2	CDPK1 IC_{50} (nM)	Parasite EC_{50} (nM)	Src IC_{50} (nM)	Microsome (min)	clogP
2		9.99	497	>10,000	15.7	3.57
11		190.6	>10,000	>10,000	>60	1.45
12		118.6	4091	>10,000	>60	2.01
13		14.15	437	>10,000	>60	2.57
14		73.09	1821	>10,000	>60	2.57
15		271.9	>10,000	>10,000	14	2.80
16		218.5	2653	>10,000	14	2.59

B

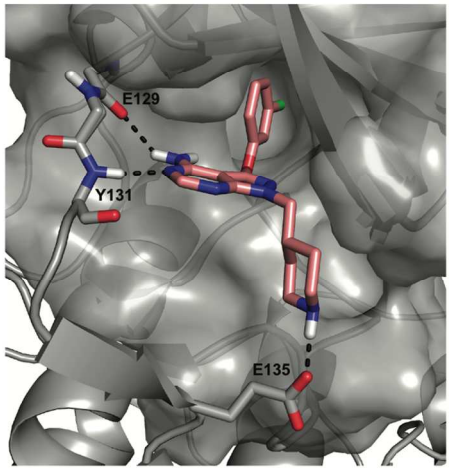

Figure 2

152x79mm (300 x 300 DPI)

A

Compound #	R_1	Y	R_2	CDPK1 IC_{50} (nM)	Parasite EC_{50} (nM)	Src IC_{50} (nM)	Microsome (min)	clogP
13		N		14.15	437	>10,000	>60	2.57
17		N		14.53	799	>10,000	>60	2.31
18		N		19.2	242	>10,000	11	3.00
19		N		517	729	>10,000	26	2.78
20		N		16.4	3476	901	20	2.95
21		N		173	5976	>10,000	>60	1.88
22		N		67.5	2979	>10,000	>60	2.71
23		C		13.53	367	>10,000	9.6	3.82
24		N		10.9	264	>10,000	8.8	2.85
25		N		77.5	1803	>10,000	>60	3.01
26		N		95.3	>10,000	>10,000	>60	1.22
27		N		10.2	1004	>10,000	11	3.45
28		N		47	1000	>10,000	2.5	3.28

B

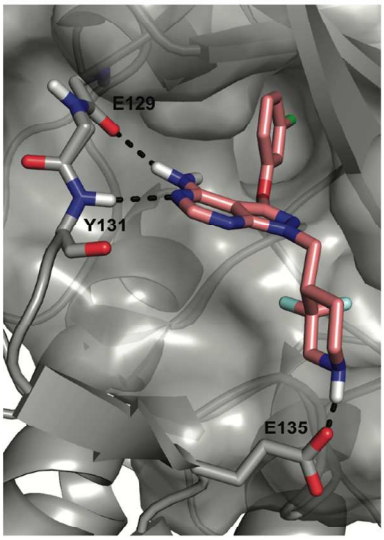

Figure 3

177x143mm (300 x 300 DPI)

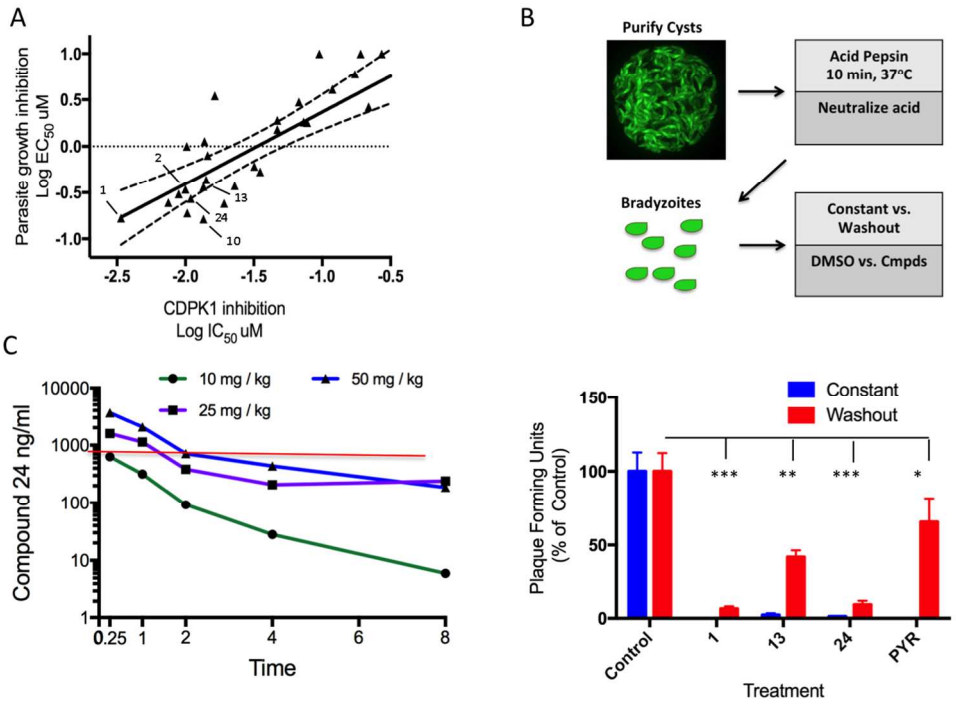

Figure 4

177x133mm (300 x 300 DPI)

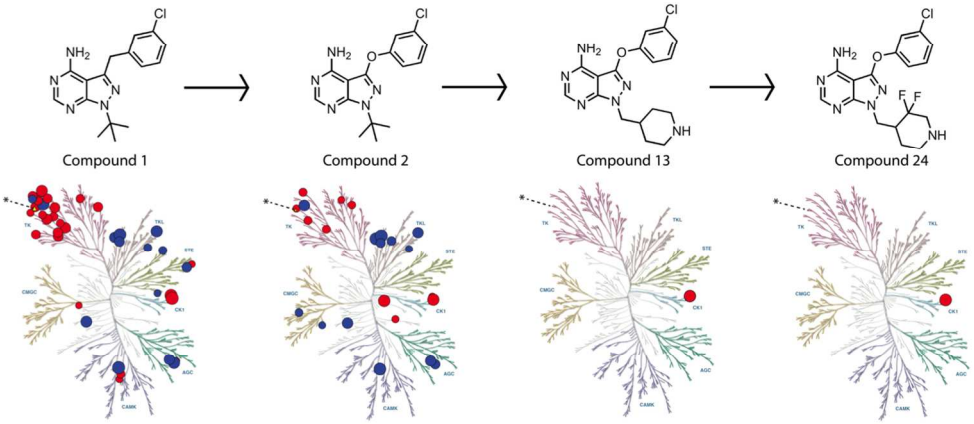

Figure 5

152x79mm (300 x 300 DPI)

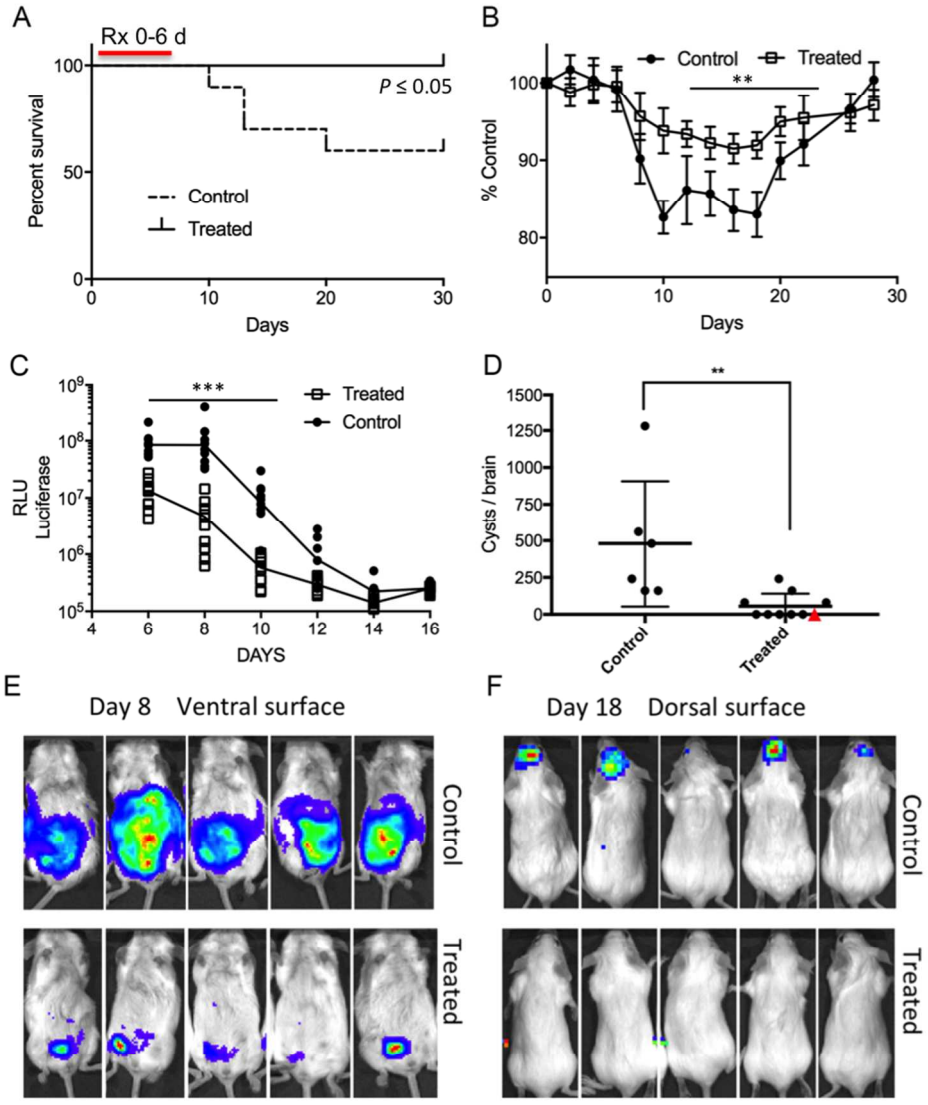

Figure 6

177x208mm (300 x 300 DPI)

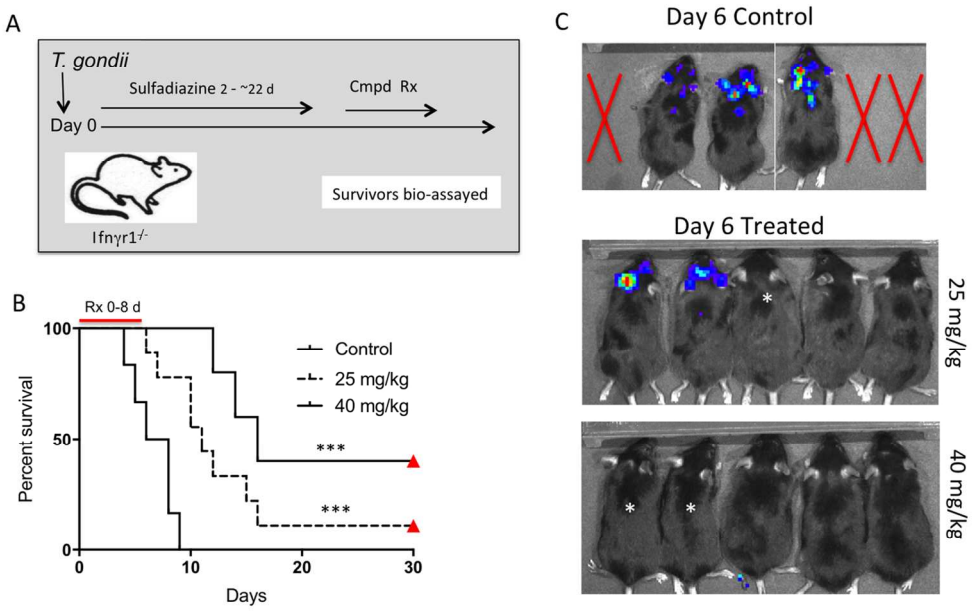

Figure 7

177x117mm (300 x 300 DPI)